Measurement Report: Cloud condensation nuclei (CCN) activity in the South China Sea from shipborne observations during summer and winter of 2021: seasonal variation and anthropogenic influence.

Hengjia Ou[1], Mingfu Cai[2], Yongyun Zhang[1], Xue Ni[1], Baoling Liang[3], Qibin Sun[4,5], Shixin Mai[1], Cuizhi Sun[6], Shengzhen Zhou[1], Haichao Wang[1], Jiaren Sun[2], Jun Zhao[1]

[1]School of Atmospheric Sciences, Guangdong Province Key Laboratory for Climate Change and Natural Disaster Studies, Southern Marine Science and Engineering Guangdong Laboratory (Zhuhai), Sun Yat-sen University, Zhuhai, Guangdong 519082, China

[2]Guangdong Province Engineering Laboratory for Air Pollution Control, Guangdong Provincial Key Laboratory of Water and Air Pollution Control, South China Institute of Environmental Sciences, MEE, Guangzhou 510655, China

[3]Guangzhou Sub-branch of Guangdong Ecological and Environmental Monitoring Center, Guangzhou 510006, China

[4]Dongguan Meteorological Bureau, Dongguan, Guangdong, 523086, China

[5]Dongguan Engineering Technology Research Center of Urban Eco-Environmental Meteorology, Dongguan, Guangdong, 523086, China

[6]Southern Marine Science and Engineering Guangdong Laboratory (Zhuhai), Zhuhai, Guangdong 519082, China

Correspondence: Mingfu Cai (caimingfu@scies.org) and Jun Zhao (zhaojun23@mail.sysu.edu.cn)

Abstract

Understanding seasonal variations in cloud condensation nuclei (CCN) activity and the impact of anthropogenic emissions in marine environments is crucial for assessing climate change. This study presents findings from two shipborne observations conducted in the South China Sea (SCS) during the summer and winter of 2021. In the summer, higher particle number concentrations but lower mass concentrations of non-refractory submicron particle matters (NR-PM_1) were observed. This was attributed to the dominance of particles in the Aitken mode during summer, whereas there was a more balanced distribution of Accumulation mode and Aitken mode particles in winter. Summer particles were more hygroscopic, exhibiting higher activation ratios (ARs) at high supersaturation (SS) levels, while hygroscopicity at low SS was similar in both seasons. During the summer, three distinct periods were identified based on the air mass sources: terrestrial air masses from Luzon Island ("Luzon" period), and from the Indochinese Peninsula ("Indochinese Peninsula" period), and marine air masses. In winter, the periods were defined by terrestrial air masses from Mainland China ("Mainland China" period), a mix of Mainland China and marine air masses ("Mixed" period), and purely marine air masses. The "Luzon" period in summer exhibited the highest particle number concentration, especially in the Aitken mode, resulting in the highest CCN number concentration (N_{CCN}). Aerosol hygroscopicity was higher during the "Indochinese Peninsula" period compared to the "Luzon" period, leading to a higher AR due to the combination of higher hygroscopicity and a greater fraction of accumulation mode particles. The "Mainland China" period in winter showed a high nitrate fraction in NR-PM_1, but the inorganic fraction was similar to it in “Luzon” period, resulting in comparable hygroscopicity at low SS to the "Luzon" period. However, hygroscopicity at small particle sizes was much lower in the "Mainland China" period than in the summer periods. The "Mixed" period in winter exhibited a higher fraction of accumulation mode particles, causing a higher AR compared to the "Mainland China" period. CCN closure analysis, considering aerosol composition and mixing state, revealed that summer aerosol was primarily internally mixed, whereas smaller aerosol in winter was primarily externally mixed. The potential effect of undetected sea salt may lead to an underestimation of aerosol hygroscopicity in summer. This study highlights significant seasonal differences in aerosol properties and the impact of different types of terrestrial air masses on CCN activity in the SCS, contributing to our understanding of regional climate influences.

1.Introduction

Aerosols can act as cloud condensation nuclei (CCN), influencing cloud formation, lifespan, and albedo, thus indirectly impacting global radiative balance (Fletcher et al., 2011; Albrecht, 1989). The aerosol-cloud interaction currently represents the largest uncertainty in radiative forcing within climate models, ranging from -1.7 to -0.3 W m^{-2} (IPCC, 2021). This uncertainty can be attributed to the significant spatiotemporal variability in the aerosol size distribution and the ability of atmospheric aerosol particles acting as CCN (CCN activity) (Fitzgerald, 1973). Thus, field measurements of aerosol size distribution and physicochemical properties are needed to better understand the radiative forcing exerted by atmospheric aerosol particles.

Previous studies suggest that particle number size distribution (PNSD) is a primary factor influencing CCN concentrations (Dusek et al., 2006; Rose et al., 2010; Pöhlker et al., 2016; Burkart et al., 2011). The PNSD can account for 84–96% of the variability in CCN concentrations (N_{CCN}) (Dusek et al., 2006), while CCN activities may also play a significant role in CCN concentrations (Quinn et al., 2008; Cai et al., 2018; Ovadnevaite et al., 2017; Liu et al., 2018; Crosbie et al., 2015), which are primarily governed by the particle size, chemical composition, mixing state, surface tension, and hygroscopicity (Köhler, 1936; Seinfeld and Pandis, 2016). Among these factors, the impact of hygroscopicity on CCN activities has received great attention in recent years (Petters and Kreidenweis, 2007; Ajith et al., 2022; Rose et al., 2010). Petters and Kreidenweis (2007) proposed the κ- Köhler theory based on the Köhler theory to quantify the ability of aerosol particles to absorb moisture and become CCN based on the aerosol hygroscopicity parameters (κ). Ajith et al. (2022) showed that 64% of particles can be activated as CCN when κ is equal to 0.37, whereas when κ decreases to 0.23, only 48% of particles can be activated in the tropical coastal area.

Significant seasonal variations in PNSD and hygroscopicity under both terrestrial and marine environments were observed in previous field observations, leading to the seasonal variations in N_{CCN} (Crosbie et al., 2015; Schmale et al., 2018; Burkart et al., 2011; Bougiatioti et al., 2009; Sihto et al., 2011; Leena et al., 2016; Ross et al., 2003; Gras and Keywood, 2017; Quinn et al., 2019). Crosbie et al. (2015) revealed that in the urban area of Arizona particles had larger sizes, higher hygroscopicity, and N_{CCN} was also higher during winter, while a higher abundance of smaller particles was observed during summer owing to stronger photochemical reactions. In pristine environments like mountain, coastal, and forested

regions, seasonal variations in N_{CCN} and PNSD were more pronounced than urban and rural areas (Schmale et al., 2018). Pöhlker et al. (2016) observed significant differences in N_{CCN} between the wet and dry seasons in the Amazon rainforest, while the κ values remained relatively stable. They also noted increased particle concentrations and aerosol hygroscopicity, both subject to the impact of long-range transport originating from anthropogenic emissions. Observations in marine areas during different seasons are relatively scarce compared with those in inland areas. Gras (1995) found that both particle concentration and N_{CCN} in the Southern Ocean reached their peaks during summer and gradually decrease to their valleys in winter. Quinn et al. (2019) showed that sea spray aerosols make a relatively significant contribution to N_{CCN} only during winter in the Western North Atlantic, while in other seasons, the primary contribution comes from biogenic aerosols oxidized from dimethyl sulfide (DMS). Zheng et al. (2020) revealed that sulfate dominates the particle condensational growth to CCN sizes during summer in the North Atlantic, while secondary organic aerosols played a significant role in particle growth throughout all seasons. These results indicate that CCN activity and concentration could vary in a large range during different seasons. Thus, further observations across different seasons in marine environments are needed to enhance our understanding of marine CCN activities and their seasonal variations.

The South China Sea (SCS), located in Southeast Asia and bordered by China, the Indochinese Peninsula, and Maritime Southeast Asia, is significantly influenced by air pollutants transported through terrestrial air masses. Studies have shown that these pollutants play a crucial role in determining aerosol concentration and properties in the region (Atwood et al., 2017; Xiao et al., 2017; Geng et al., 2019; Liang et al., 2021; Sun et al., 2023; Qin et al., 2024). For instance, Xiao et al. (2017) reported that 69.7% of nitrate and 57.5% of sulfate in the SCS originated from fossil fuel combustion, particularly coal burning in Chinese coastal regions. Additionally, Liang et al. (2021) and Sun et al. (2023) observed an increase in the organic fraction and concentration of submicron aerosols when the region was influenced by terrestrial air masses from Mainland China and the Indochinese Peninsula in the northern SCS. Further studies highlighted the variation in aerosol properties under different air mass influences. Atwood et al. (2017) found a significant bimodal particle distribution with a κ value of 0.65 in the southern SCS under marine air mass influence, whereas a unimodal distribution with a κ of 0.4 was observed under continental air mass influence.

The SCS experiences a typical monsoon climate with distinct seasonal wind direction changes (Wang et al., 2009). The northeast monsoon, occurring from November to March, is characterized by

stronger average wind speeds and longer period compared to the southwest monsoon, which dominates from June to August. The transitional periods occur from April to May and September to October. During the northeast monsoon, air pollutants are primarily transported to the SCS by terrestrial air masses from China (Xiao et al., 2017; Liu et al., 2014; Geng et al., 2019). In contrast, during the summer, pollutants mainly originate from terrestrial air masses from the Indochinese Peninsula and Maritime Southeast Asia (Geng et al., 2019; Liang et al., 2021; Sun et al., 2023). These varying sources of anthropogenic emissions exerts different impacts on CCN activity differently across seasons. Additionally, the high cloud fraction over the SCS varies from approximately 0.3 to 0.7 across different months, indicating that aerosol-cloud interactions in the region may differ between seasons (Lu et al., 2022). However, due to limited observational data, our understanding of seasonal variations in CCN activity in the SCS remains incomplete. Conducting comprehensive observational studies on CCN activity across different seasons is essential for improving our understanding of aerosol-cloud interactions on the SCS.

In this study, we conducted two shipborne observations in the SCS during summer (May 5–June 9, 2021) and winter (December 19–29, 2021). Our observations with online instruments focused on measuring aerosol chemical composition, PNSD, and CCN activation in the region. Our results provide valuable insights into the differences in CCN activity between winter and summer, as well as the influence of different types of terrestrial air masses on CCN activity in the SCS across different seasons.

2. Methodology

2.1 Cruise information and onboard measurements

2.1.1 Cruise information

This study consists of two research cruises conducted during the summer and winter of 2021, respectively. These two cruises were interdisciplinary scientific expeditions, integrating fields such as marine geology, oceanography, and atmospheric environment. The primary objective in atmospheric environment was to investigate the impact of different monsoons on the atmospheric environment of the South China Sea (SCS). The summer and winter cruises were carried out respectively by the vessels "Tan Kah Kee" and "Sun Yat-sen University". The "Tan Kah Kee" is an oceanographic research vessel with a length of 77.7 meters, a beam of 16.24 meters, and a displacement of 3611 tons. The "Sun Yat-sen University" is a comprehensive oceanographic training vessel with a total length of 114.3 meters, a beam of 19.4 meters, and a displacement of 6880 tons.

The first cruise was from May 5th to June 9th, 2021. The cruise started from Xiamen Port and traversed from the northern to the central-southern South China Sea, and then circled back near Hainan Island, and finally returned to Xiamen Port. The second cruise was from December 19th to December 29th, 2021. It began from Gaolan Port in Zhuhai and reached the vicinity of Yongxing Island, and ultimately returned to Gaolan Port (Fig. 1a). Unfortunately, due to adverse weather conditions, such as strong winter monsoon winds causing poor sea conditions, and the fact that it was the first scientific deployment of the research vessel Sun Yat-sen University, the winter cruise had a shorter duration and covered a narrower spatial range compared to the summer cruise. On both cruises, most of the instruments were housed in a single compartment and the sampling lines were extended from the window of the compartment to the height of the ship's bridge (Fig. 1a).

2.1.2 Size-resolved cloud condensation nuclei activity measurement

The size-resolved CCN activity was measured with a combination of a scanning mobility particle sizer (SMPS) system and a cloud condensation nuclei counter (model CCNc-200, DMT Inc., USA), the scanning mobility CCN analysis (SMCA) method initially proposed in Moore et al. (2010). The SMPS system consisted of a differential mobility analyzer (DMA; model 3082, TSI., Inc.) and a condensation particle counter (CPC; model 3756, TSI Inc.). The SMPS and the CCNc system were used to measure PNSD and size-resolved CCN number concentration at a mobility size range of 10–500 nm and 10–593 nm in summer and winter campaign, respectively.

The supersaturation (SS) of the CCNc was set at 0.2 %, 0.4 %, and 0.7 % in summer campaign and 0.1%, 0.2 %, 0.4 %, and 0.7 % in winter campaign, respectively. Before the measurements, the CCNc was calibrated with ammonium sulfate ($(NH_4)_2SO_4$) particles at each set SS. Detailed description of the instrument configuration and calibration can be found in Cai et al. (2018).

2.1.3 Aerosol chemical composition measurement

The chemical composition of atmospheric non-refractory submicron particulate matter (NR-PM_1), including sulfate, nitrate, organics, ammonium, and chloride, was measured using an online time-of-flight ACSM (ToF-ACSM; Aerodyne Inc., USA). The sampling time of the ToF-ACSM was approximately 10 min. The relative ionization efficiency (RIE) values of the instrument were calibrated using ammonium nitrate (NH_4NO_3) and ammonium sulfate ($(NH_4)_2SO_4$) both before the start and after

the completion of the campaigns. The RIE values for ammonium were 3.31 and 3.33 during the summer and winter, respectively, while the ones for sulfate were 1.02 and 0.81 during the summer and winter, respectively. The collection efficiency (CE) was determined as shown in Sun et al. (2023) and time-independent CE values were used in this study. Detailed CE calculation can be found in the supplementary (Text S1, and Fig. S1). The organic carbon (OC)/elemental carbon (EC) concentrations in $PM_{2.5}$ were measured using a semi-continuous OC/EC analyzer (Model-4, Sunset Laboratory Inc., USA) based on the thermal optical transmittance technique and detailed measurement process can be found in Sun et al. (2023). The black carbon concentrations were measured with an aethalometer (AE33, Magee Scientific).

2.1.4 Trace Gas and meteorological parameter measurements

The concentrations of trace gases (CO, O_3, SO_2, and NOx) were measured using gas monitors (T400U, T100U, and T200U; Teledyne API Inc., USA). The meteorological elements, including temperature, relative humility, wind speed, and wind direction, were measured by the combined automatic weather station onboard the vessels. During the winter cruises, meteorology data before 12.22 was missed due to the calibration for the automatic weather station before 12.22. The timeseries of meteorological data were presented in Fig. S2.

2.2 Data analysis

2.2.1 CCN activation

The size-resolved number concentration of total praticle and cloud condensation nuclei were obtained from the SMPS and CCNc thourgh the SMCA method. The activation diameter was determined by fitting the activation ratio (AR, N_{CCN}/N_{CN}) and dry diameter at each supersaturation through the following equation:

$$AR = \frac{B}{1+\left(\frac{D_P}{D_{50}}\right)^C}, \quad (1)$$

where AR is the size-resolved AR, D_P represents dry particle diameter (nm); B, C, and D_{50} are the three fitting parameters, representing the asymptote, the slope, and the inflection point of the sigmoid, respectively (Moore et al., 2010). The D_{50} parameter, also known as the critical diameter, corresponds to the particle size at which 50% of the particles are activated at a specific SS. The fitting results from SMCA method measured in this study are presented in Fig. S3.

196 The hygroscopicity parameter (κ) which represents CCN activity according to κ-Köhler equation is
197 calculated as follows (Petters and Kreidenweis, 2007):

198 $$\kappa = \frac{4A^3}{27{D_{50}}^3(lnS_c)^2},\ A = \frac{4\sigma_{s/a}M_w}{RT\rho_w} \quad (2)$$

199 where ρ_w is the density of pure water (about 997.04 kg m^{-3} at 298.15 K), M_W is the molecular weight of
200 water (0.018 kg mol^{-1}), $\sigma_{s/a}$ corresponds to the surface tension of the solution-air interface and is assumed
201 to be equal to the surface tension of pure water ($\sigma_{s/a}$=0.0728 N m^{-1} at 298.15 K), R is the universal gas
202 constant (8.314 J mol^{-1} K^{-1}), T denotes thermodynamic temperature in kelvin (298.15 K), and D_{50} is the
203 critical diameter (in m).

204 **2.2.2 Closure Method**

205 According to Petters and Kreidenweis. (2007), κ can be predicted by a simple mixing rule based
206 on chemical volume fractions:

207 $$\kappa_{sim} = \sum_i \varepsilon_i \kappa_i \quad (3)$$

208 where ε_i and κ_i are the volume fraction and hygroscopicity parameter for the specific dry component in
209 the mixture. We obtained ε from aerosol chemical composition measured by the ToF-ACSM. In this study,
210 κ from $(NH_4)_2SO_4$ (0.48), NH_4NO_3 (0.58), and Nacl (1.1) represent the κ of SO_4^{2-}, NO_3^-, and Cl^- provided
211 by the ToF-ACSM (Huang et al., 2022). Besides, the κ of organic was 0.1 at this study. The density of
212 $(NH_4)_2SO_4$, NH_4NO_3, Nacl and organic are 1769 kg m^{-3}, 1720 kg m^{-3},2165 kg m^{-3}, and 1400 kg m^{-3}
213 (Huang et al., 2022; Gysel et al., 2007).

214 **2.2.3 CCN concentration and activation ratio calculation**

215 The CCN concentration (N_{CCN}) can be predicted based on particle number size distribution (PNSD)
216 and D_{50} at a specific SS. It can be calculated by the following equation (Cai et al., 2018):

217 $$N_{CCN}(SS) = \int_{D_{50}(SS)}^{\infty} N_{CN}\,(D_P)dD_p \quad (4)$$

218 where N_{CCN} (SS) is CCN concentration at a specific SS, D_{50}(SS) is the activation diameter at a specific
219 SS from the SMCA method or from closure method and $N_{CN}(D_P)$ is the particle number concentration
220 under specific diameter from SMPS measurement.

221 The AR can be calculated by:

222 $$AR = \frac{\int_{D_{50}(SS)}^{\infty} N_{CN}(D_P)dD_p}{\int_0^{\infty} N_{CN}(D_P)dD_p} \quad (5)$$

It is noting that the AR here is bulk AR.

To investigate the impact of the fraction and mixing state of aerosol on N_{CCN}, two CCN simulation scheme are applied in this study (Patel et al., 2021).

(1) Internal-mixed scheme: the aerosol composition from the Tof-ACSM was assumed to be size-independent and internally mixed. All aerosol has an identical chemical compostion in the whole size range. N_{CCN} is calculated by $_{Ksim}$ and measured PNSD according to Eq. (2), Eq. (3), and Eq. (4).

(2) External-mixed scheme: the aerosol composition from the Tof-ACSM was assumed to be size-independent and externally mixed. Four type of aerosol ($(NH_4)_2SO_4$, NH_4NO_3, Nacl and organic) are assumed to have identical concentration at each size. N_{CCN} is calculated according to the Eq. (4)

To access the simulation result from these two schemes, normalized mean bias (NMB) was used in this study:

$$NMB = \frac{\sum(N_{CCN,sim} - N_{CCN,obs})}{\sum N_{CCN,obs}} \quad (6)$$

where $N_{CCN,sim}$ is the simulated N_{CCN} from two schemes, and $N_{CCN,obs}$ is the observed N_{CCN}.

2.2.4 Backward trajectory simulation and cluster analysis

Backward trajectory calculations were performed using MeteoInfo, an open-source software (Wang, 2014) to determine potential source origins. Weekly GDAS1 (Global Data Assimilation System at a resolution of 1°) files were downloaded from the NOAA Air Resource Laboratory (ARL) website (https://www.ready.noaa.gov/gdas1.php). The calculation of backward trajectories is performed every 1hour based on the location mentioned below, generating 72-hour backward trajectories at 500m.

To clarify the sources of air masses, we applied cluster analysis in this study. During the summer cruise, we conducted cluster analysis at two key locations: the midpoint of the ship's track before the outbreak of the summer monsoon (May 5-23) and the midpoint of the track after the summer monsoon began (May 24-June 9). In the winter cruise, cluster analysis was performed at two specific locations: the ship's anchorage near Big Ten-thousand Mountain Island (December 19-22 and December 27-29) and the midpoint between Dawan Mountain Island and Yongxing Island (December 23-26).

2.2.5 Data quality control

To ensure reliable atmospheric samples in the SCS and mitigate the influence of research vessel emissions, we applied the following data processing procedures (Huang et al., 2018; Cai et al., 2020; Liang et al., 2021).

Firstly, we identified organic compounds, black carbon (BC), and small particulate matter (41.4 nm particles) as indicators of ship emissions, recognizing their sudden peak values as indicative of the ship's own emissions.

Secondly, we accounted for the relative positions of the ship's chimney and the sampling tube. During the summer cruise, we excluded data corresponding to a relative wind direction (with respect to the ship's bow) between 150° and 270° and a relative wind speed (with respect to the ship's speed) of less than 2.5 m s^{-1} (Fig. S4a, Fig. S5a1, and Fig. S6a-c). During the winter cruise, we excluded data for a relative wind direction between 150° and 220° and a relative wind speed of less than 2.5 m s^{-1} (Fig. S4b, Fig. S5b1, and Figs. S6d-f).

Applying these criteria, 74.8% of the data in summer and 92.2% in winter (both at 10-minute resolution) were classified as “clean” and retained for analysis. The timeseries of data before and after quality control is shown in Fig. S7.

3. Results and discussion

3.1 CCN concentration and aerosol characteristics over SCS in summer and winter

Figure 2 presented the timeseries of PNSD (a1 and a2), NR-PM_1 mass concentrations and fractions (b1 and b2, c1 and c2), number concentrations of CCN (d1 and d2), and hygroscopicity κ-values (e1 and e2) during two campaigns in summer and winter. During the summer cruise, we observed two distinct periods around the onset of the summer monsoon. The South China Sea (SCS) summer monsoon began in the sixth pentad of May (Chao et al., 2022). In winter, the influence of the winter monsoon persisted throughout the entire observation period (Fig. 1c). Despite our measurements being limited to the northern SCS in winter, the impact of the Northeast Monsoon on the SCS was evident.

The average particle number concentration in summer (6966 cm^{-3}) was higher than in winter (4988 cm^{-3}), primarily due to the higher number concentration of Aitken-mode particles in summer (Fig. 3a-b). In summer, particles were concentrated in smaller sizes, whereas in winter, particle size distribution was

relatively balanced between the Aitken mode (2185 cm^{-3}) and the accumulation mode (2176 cm^{-3}) (Fig. 3a-b).

The average mass concentration of NR-PM_1 was 3.76 μg m^{-3} in summer and increased to 9.39 μg m^{-3} in winter (Fig. 3c-d). In summer, the dominant aerosol component was sulfate (45.5%), followed by organics (35.8%), ammonium (12.9%), nitrate (4.0%), and chloride (1.9%) (Fig. 3c), similar to the pattern observed in the northern SCS during the summer of 2018 (Fig. 3e) (Liang et al., 2021). However, in winter, organics became the predominant aerosol component (37%), with nitrate (22.2%) replacing sulfate (18.9%) as the highest proportion of inorganic components (Fig. 3d).

The average number concentration of cloud condensation nuclei (N_{CCN}) in summer was higher than in winter at all supersaturation (SS) levels (Table 1). The absolute difference in the N_{CCN} between summer and winter was greater at high SS (ΔN_{CCN}=2099 cm^{-3} and 1865 cm^{-3} at 0.4% SS and 0.7% SS, respectively) compared to low SS (ΔN_{CCN}=341 cm^{-3} at 0.2% SS), likely due to the significant difference in Aitken-mode particles between the two seasons (Fig. 3a-b).

Aerosol hygroscopicity (κ) was similar at low SS but differed significantly at high SS between summer and winter (Table 1). The hygroscopicity pattern varied between seasons: in summer, κ increased with SS (from 0.49 to 0.72 between 0.2% SS and 0.4% SS), while in winter, κ decreased with SS (from 0.50 to 0.15 between 0.1% SS and 0.7% SS) (Fig. 3a-b). The winter κ pattern was similar to observations in the Western North Pacific (Table 1) (Kawana et al., 2020). Additionally, the winter κ values were comparable to those in Guangzhou, adjacent to the SCS, indicating that the northern SCS is influenced by air masses from Mainland China under the significant influence of the Northeast Monsoon during winter.

3.2 Anthropogenic influence on CCN concentration in different season

Based on cluster analysis, we identified periods affected by different types of air masses. In summer, three terrestrial air mass sources were confirmed: from Luzon Island (referred to as “Luzon”), Palawan Island, and the Indochinese Peninsula, along with a marine air mass source (Fig. 4a). Due to the small fraction of air masses from Palawan Island, this period was excluded from the study. Consequently, the periods affected by air masses from Luzon, the Indochinese Peninsula, and marine sources were referred to as the “Luzon” period, “Indochinese Peninsula” period, and “Marine-s” period, respectively. In winter, the identified air mass sources included Mainland China, a Mainland China-SCS mixed source (referred

307 to as “Mixed”), and a marine source (Fig. 4b). These were named as the “Mainland China” period,
308 “Mixed” period, and “Marine-w” period, respectively.

309 Terrestrial air masses significantly affected the marine atmosphere in the SCS, resulting in higher
310 NR-PM_1 mass concentration and a higher fraction of organic compounds compared to those influenced
311 by marine air masses (Fig. 5). Additionally, the number concentration of particles (N_{CN}) in the
312 accumulation mode and the number concentration of cloud condensation nuclei (N_{CCN}) at low
313 supersaturation (SS) were higher during periods influenced by terrestrial air masses than those during
314 marine air mass periods (Table 2).

315 In summer, the “Luzon” period had the highest N_{CN}, particularly in the Aitken mode, among all
316 periods in both summer and winter (Fig. 6a and Table 1). The high fraction of Aitken mode particles
317 contributed to the lowest activation ratio (AR) among the summer periods (Fig. 7a), further exacerbated
318 by low hygroscopicity during this period (Fig. 7b). This high fraction of Aitken mode particles likely
319 indicates a high fraction of primary organic aerosol, which lowers aerosol hygroscopicity.

320 The N_{CN} during the “Indochinese Peninsula” period was lower than during the “Marine-s” period
321 (Table 2). This difference was mainly due to the variation of Aitken mode particles, while accumulation
322 mode particles were higher during the “Indochinese Peninsula” period than in “Marine-s” period (Table
323 2). The “Marine-s” period occurred primarily during the transition before the summer monsoon onset,
324 when wind direction shifted from east (Luzon Island direction) to southwest (Indochinese Peninsula
325 direction). Anthropogenic emissions from Luzon Island still affected the marine atmosphere, leading to
326 higher concentrations of Aitken mode particles compared to the “Indochinese Peninsula” period (Table
327 2). The higher fraction of accumulation mode particles and higher hygroscopicity during the
328 “Indochinese Peninsula” period resulted in a higher AR compared to the “Luzon” period. Despite a higher
329 organic fraction in NR-PM_1 during the “Indochinese Peninsula” period (Fig. 5), hygroscopicity was still
330 higher due to a higher oxidation degree of organics, indicated by a higher m/z 44 to 43 ratio (5.87
331 compared to 5.60 in the “Luzon” period) (Lambe et al., 2011; Jimenez et al., 2009). Additionally, higher
332 wind speeds during this period (7.26 m s^{-1} compared to 3.18 m s^{-1} in the “Luzon” period) leaded a higher
333 fraction of sea salt (Huang et al., 2022), resulting a higher aerosol hygroscopicity. Unfortunately, owing
334 to instrument limit, sea salt cannot be detected by the ToF-ACSM.

335 In winter, nitrate had the highest fraction in NR-PM_1 (25.4%) during the “Mainland China” period
336 among other periods. Due to similar hygroscopicity between nitrate and sulfate and similar inorganic

fractions between the "Mainland China" and "Luzon" periods, κ at 0.2% SS was comparable (0.30 and 0.33, respectively) (Fig. 7b). However, aerosol hygroscopicity at small sizes was much lower in the "Mainland China" period than in the "Luzon" period (Fig. 7b), contributing to the low AR in the "Mainland China" period (Fig. 7a). This lower hygroscopicity could be due to lower sulfate concentration, oxidized by DMS, in winter than in summer, as higher sea surface temperatures in summer (29.3°C) compared to winter (18.0°C) promote DMS production by phytoplankton (Bates et al., 1987). The similar fractions of Aitken mode and accumulation particles indicated that PNSD could not fully explain the low AR in the "Mainland China" period. Lower N_{CN} and AR in the "Mainland China" period compared to the "Luzon" period resulted in a lower N_{CCN}.

During the "Mixed" period, the N_{CCN} was lower than in the "Mainland China" period, attributed to decreased N_{CN} (Table 2). However, particles were primarily concentrated in the accumulation mode, distinct from other terrestrial air mass periods (Fig. 6), leading to a significantly higher AR than the "Mainland China" period. Organic aerosol hygroscopicity was higher during the "Mixed" period than the "Mainland China" period, supported by a higher m/z 44 to 43 ratio (3.88 compared to 3.10 in the "Mainland China" period), explaining the higher hygroscopicity despite a higher organic fraction in NR-PM_1. Additionally, lower BC concentration in the "Mixed" period (1.20 μg m^{-3} compared to 2.25 μg m^{-3} in the "Mainland China" period) suggested a lower fraction of BC, which was hydrophobic. Higher wind speeds in the "Mixed" period (10.77 m s^{-1} compared to 7.14 m s^{-1} in the "Mainland China" period) could increase sea salt fraction, further enhancing aerosol hygroscopicity.

3.3 CCN closure analysis

CCN closure study was widely applied to investigate the impacts of different factors on the CCN activity (Patel et al., 2021; Cai et al., 2018; Meng et al., 2014; Deng et al., 2013). In this study, two schemes considering aerosol composition and mixing state based on CCN closure method mentioned in 2.2.3 were applied. The fitting parameter and coefficient of determination (R^2) was shown in Table 3 and the fitting plots from two schemes were shown in Fig. S8 and Fig. S9. Besides, the NMB from these two schemes was presented in Fig. 8.

In summer, the NMB always lower than 0, which indicated that simulated aerosol hygroscopicity was lower than observed value (Fig. 8). Sea salt which cannot be detected by the ToF-ACSM may account for higher fraction in summer due to low aerosol concentration in summer (Fig. 3c), resulting in

the underestimation of aerosol hygroscopicity. The NMB exhibits different trends with changes in SS in "Luzon" and "Indochinese Peninsula" period. Better fitting result appeared in high SS in "Indochinese Peninsula" period, while it appeared in low SS in "Luzon" period (Fig. 8), which indicated that aerosol fraction had different trend as particle size increased in these two periods. Besides, "Internal-mixed" scheme had more precious result than it in "External-mixed" scheme in summer (Fig. 8), suggesting the aerosol was primary internally mixed in summer.

In winter, the "External-mixed" scheme always showed a better result than "Internal-mixed" scheme at high SS (0.4% SS and 0.7% SS), indicating that particles in small size were mainly externally mixed. Considering the low hygroscopicity of small-sized particles in winter, it is likely that a significant fraction of these particles consists of externally mixed BC, which probably originated from fresh anthropogenic emissions and remains unmixed with other inorganic salts and organics. As BC ages, inorganic and organic components adhere to it, which would lead to the increase of diameter and particles tended to be internally mixed (Sarangi et al., 2019). This transition resulted in higher hygroscopicity in large-sized particle compared to the smaller-sized particles. Besides, overestimation of aerosol hygroscopicity at high SS could be owing to a higher fraction of non- or less- hygroscopic component (such as organic and BC) at small particle sizes. The predicted N_{CCN} at 0.1% SS are 10%-20% lower than the observed concentrations, whereas the predicted value at 0.2% SS more closely aligns with the observed concentrations (Fig. 8). It could be owing to the higher fraction of sea salt at larger particle size. However, due to instrument limitations, black carbon and sea salt cannot be detected by the ToF-ACSM. More observations containing sea salt and black carbon are needed in the future to better assess their effects on aerosol hygroscopicity in SCS. In addition, further study size-resolved aerosol composition can also enhance the understanding on CCN activity in the SCS.

4. Conclusion

In this study, we investigated the seasonal variations of cloud condensation nuclei (CCN) activity in the South China Sea (SCS) and explored the impact of anthropogenic emissions. Shipborne observations were conducted during the summer (May 5–June 9) and winter (December 19–29) of 2021. We measured CCN activity, chemical composition, and particle number size distribution (PNSD) using several onboard instruments, including a ToF-ACSM, a CCNc, an SMPS, and an AE33. Observations

included periods before and after the summer monsoon outbreak and periods influenced by the winter monsoon.

Our results show that particle number concentration (N_{CN}) and CCN number concentration (N_{CCN}) were higher in summer than in winter, while the mass concentration of non-refractory submicron particulate matter (NR-PM_1) was lower in summer. This can be attributed to the predominance of Aitken mode particles in summer, compared to the higher concentration of accumulation mode particles in winter. Additionally, aerosol hygroscopicity and activation ratio (AR) were found to be higher in summer than in winter.

Backward trajectory and cluster analysis identified distinct air mass influences. In summer, we confirmed periods affected by terrestrial air masses from Luzon Island ("Luzon" period) and the Indochinese Peninsula ("Indochinese Peninsula" period), as well as a period influenced by marine air masses ("Marine-s" period). In winter, the periods were influenced by terrestrial air masses from Mainland China ("Mainland China" period), mixed air masses from Mainland China and marine sources ("Mixed" period), and marine air masses ("Marine-w" period). Periods influenced by terrestrial air masses showed higher NR-PM_1 mass concentration, organic fraction, and N_{CCN}, especially at low supersaturation (SS), compared to those influenced by marine air masses.

During the "Luzon" period, high N_{CCN} was observed, attributed to high N_{CN}, especially in the Aitken mode. This high concentration in the Aitken mode resulted in a low AR at 0.2% SS, indicating a higher fraction of primary organic aerosol with low hygroscopicity. This caused lower overall hygroscopicity compared to other summer periods. The lower ratio of m/z 44 to 43 also suggested a lower oxidation degree of organics in this period. In the "Indochinese Peninsula" period, a higher particle fraction in the accumulation mode compared to the "Luzon" period led to a higher AR, combined with increased hygroscopicity.

In winter, the "Mainland China" period showed a high nitrate fraction in NR-PM_1. Similar inorganic fractions in NR-PM_1 between the "Mainland China" and "Luzon" periods resulted in similar aerosol hygroscopicity at low SS (0.2% SS). However, at higher SS (0.4% SS and 0.7% SS), the "Mainland China" period exhibited much lower hygroscopicity, causing a lower AR at high SS. During the "Mixed" period, accumulation mode particles predominated, leading to a high AR. This indicated an aging process during transport, with more oxidized organics and higher aerosol hygroscopicity. The lower black carbon

(BC) fraction and the higher sea salt fraction from high wind speed contributed to higher hygroscopicity in the "Mixed" period compared to the "Mainland China" period, despite the high organic fraction.

The CCN closure analysis, considering aerosol composition and mixing state, revealed that aerosols in summer were primarily internally mixed, while in winter, small-sized aerosols were primarily externally mixed. This distinction is crucial for climate models predicting N_{CCN} in the SCS. The underestimation of aerosol hygroscopicity in summer suggests that the effect of sea salt should be considered.

Our study highlights significant seasonal differences in CCN activity in the SCS and the influence of different types of terrestrial air masses. Future measurements including size-resolved aerosol composition and obtain more precise measurements of BC and sea salt are needed to better understanding CCN activity in this region. Additionally, our observation in winter focused on the CCN activity over the northern SCS, while the influence of air masses from Mainland China in remote SCS was still unclear. Further observations in remote SCS areas could help clarify the anthropogenic influence during winter under the effect of the winter monsoon.

Data availability. Data from the measurements are available at https://doi.org/10.6084/m9.figshare.25472545 (Ou et al., 2024).

Supplement. The supplement related to this article is available online at xxx.

Author contributions. **HO, MC, and JZ** designed the research. **YZ**, **XN, BL, and CS** performed the measurements. **HO, MC, QS, and SM** analyzed the data. **SZ and HW** provided useful comment on the paper. **HO, MC,** and **JZ** wrote the paper with contributions from all co-authors.

Competing interests. The authors declare that they have no conflict of interest.

Financial support. This work was supported by National Natural Science Foundation of China (NSFC) (Grant No. 42305123 and 42175115) and Basic and Guangzhou Applied Basic Research Foundation (Grant No. 2023A1515012240 and 2024A1515030221).

Acknowledgements. Additional support from the crew of the vessels "Tan Kah Kee" and "Sun Yat-sen University" is greatly acknowledged.

Reference

Ajith T. C, Kompalli, S. K., and Babu, S. S.: Role of Aerosol Physicochemical Properties on Aerosol Hygroscopicity and Cloud Condensation Nuclei Activity in a Tropical Coastal Atmosphere, ACS Earth Space Chem, 6, 1527-1542, doi:https://doi.org/10.1021/acsearthspacechem.2c00044, 2022.

Albrecht, B. A.: Aerosols, cloud microphysics, and fractional cloudiness, Science, 245, 1227-1230, doi:https://doi.org/10.1126/science.245.4923.1227, 1989.

Atwood, S. A., Reid, J. S., Kreidenweis, S. M., Blake, D. R., Jonsson, H. H., Lagrosas, N. D., Xian, P., Reid, E. A., Sessions, W. R., and Simpas, J. B.: Size-resolved aerosol and cloud condensation nuclei (CCN) properties in the remote marine South China Sea - Part 1: Observations and source classification, Atmos. Chem. Phys., 17, 1105-1123, doi:https://doi.org/10.5194/acp-17-1105-2017, 2017.

Bates, T. S., Cline, J. D., Gammon, R. H., and Kelly-Hansen, S. R.: Regional and seasonal variations in the flux of oceanic dimethylsulfide to the atmosphere, J. Geophys. Res. Oceans, 92, 2930-2938, doi:https://doi.org/10.1029/JC092iC03p02930, 1987.

Bougiatioti, A., Fountoukis, C., Kalivitis, N., Pandis, S. N., Nenes, A., and Mihalopoulos, N.: Cloud condensation nuclei measurements in the marine boundary layer of the eastern Mediterranean: CCN closure and droplet growth kinetics, Atmos. Chem. Phys., 9, 7053-7066, doi:https://doi.org/10.5194/acp-9-7053-2009, 2009.

Burkart, J., Steiner, G., Reischl, G., and Hitzenberger, R.: Long-term study of cloud condensation nuclei (CCN) activation of the atmospheric aerosol in Vienna, Atmos Environ, 45, 5751-5759, doi:https://doi.org/10.1016/j.atmosenv.2011.07.022, 2011.

Cai, M., Tan, H., Chan, C. K., Mochida, M., Hatakeyama, S., Kondo, Y., Schurman, M. I., Xu, H., Li, F., Shimada, K., Li, L., Deng, Y., Yai, H., Matsuki, A., Qin, Y., and Zhao, J.: Comparison of Aerosol Hygroscopcity, Volatility, and Chemical Composition between a Suburban Site in the Pearl River Delta Region and a Marine Site in Okinawa, Aerosol Air Qual Res, 17, 3194-3208, doi:https://doi.org/10.4209/aaqr.2017.01.0020, 2017.

Cai, M. F., Liang, B. L., Sun, Q. B., Zhou, S. Z., Chen, X. Y., Yuan, B., Shao, M., Tan, H. B., and Zhao, J.: Effects of continental emissions on cloud condensation nuclei (CCN) activity in the northern South China Sea during summertime 2018, Atmos. Chem. Phys., 20, 9153-9167, doi:https://doi.org/10.5194/acp-20-9153-2020, 2020.

Cai, M. F., Tan, H. B., Chan, C. K., Qin, Y. M., Xu, H. B., Li, F., Schurman, M. I., Liu, L., and Zhao, J.: The size-resolved cloud condensation nuclei (CCN) activity and its prediction based on aerosol hygroscopicity and composition in the Pearl Delta River (PRD) region during wintertime 2014, Atmos. Chem. Phys., 18, 16419-16437, doi:https://doi.org/10.5194/acp-18-16419-2018, 2018.

Chao, Q., Xiao, C., Li, w., Wang, L., Sun, L., Chen, X., Chen, Y., Li, Y., Gao, G., Liu, Y., Zhang, D., Ai, W., Chen, Y., Cui, T., Dai, T., Feng, A., Guo, Y., Huang, D., Jiang, Y., Li, D., Li, M., Liu, B., Liu, Y., Lv, Z., Mei, m., Wang, Q., Wang, Y., Yin, Y., Zeng, H., Zhang, Y., Zhai, J., Zhao, L., Zhi, R., Zhong, H., Zhou, X., Zhou, X., Zhu, X., and Wu, H.: China Climate Bulletin (2022), China Meteorological Administration, https://www.cma.gov.cn/zfxxgk/gknr/qxbg/202303/t20230324_5396394.html, 2022.

Choi, Y., Rhee, T. S., Collett, J. L., Park, T., Park, S.-M., Seo, B.-K., Park, G., Park, K., and Lee, T.: Aerosol concentrations and composition in the North Pacific marine boundary layer, Atmos Environ., 171, 165-172, doi:https://doi.org/10.1016/j.atmosenv.2017.09.047, 2017.

Crosbie, E., Youn, J. S., Balch, B., Wonaschutz, A., Shingler, T., Wang, Z., Conant, W. C., Betterton, E. A., and Sorooshian, A.: On the competition among aerosol number, size and composition in predicting CCN variability: a multi-annual field study in an urbanized desert, Atmos Chem Phys, 15, 6943-6958, doi:https://doi.org/10.5194/acp-15-6943-2015, 2015.

Deng, Z. Z., Zhao, C. S., Ma, N., Ran, L., Zhou, G. Q., Lu, D. R., and Zhou, X. J.: An examination of parameterizations for the CCN number concentration based on in situ measurements of aerosol activation properties in the North China Plain, Atmos. Chem. Phys., 13, 6227-6237, doi:https://doi.org/10.5194/acp-13-6227-2013, 2013.

Dusek, U., Frank, G. P., Hildebrandt, L., Curtius, J., Schneider, J., Walter, S., Chand, D., Drewnick, F., Hings, S., Jung, D., Borrmann, S., and Andreae, M. O.: Size matters more than chemistry for cloud-nucleating ability of aerosol particles, Science, 312, 1375-1378, doi:https://doi.org/10.1126/science.1125261, 2006.

Fitzgerald, J. W.: Dependence of the Supersaturation Spectrum of CCN on Aerosol Size Distribution and Composition, J Atmos Sci, 30, 628-634, doi:https://doi.org/10.1175/1520-0469(1973)030, 1973.

Fletcher, Squires, I. b. P., and Bowen, F. b. E. G.: The Physics of Rainclouds, 2011.

Geng, X. F., Zhong, G. C., Li, J., Cheng, Z. B., Mo, Y. Z., Mao, S. D., Su, T., Jiang, H. Y., Ni, K. W., and Zhang, G.: Molecular marker study of aerosols in the northern South China Sea: Impact of atmospheric

516 outflow from the Indo-China Peninsula and South China, Atmos Environ, 206, 225-236,
517 doi:https://doi.org/10.1016/j.atmosenv.2019.02.033, 2019.
518 Gras, J. L.: CN, CCN and particle size in Southern Ocean air at Cape Grim, Atmos Res, 35, 233-251,
519 doi:https://doi.org/10.1016/0169-8095(94)00021-5, 1995.
520 Gras, J. L. and Keywood, M.: Cloud condensation nuclei over the Southern Ocean: wind dependence
521 and seasonal cycles, Atmos. Chem. Phys., 17, 4419-4432, doi:https://doi.org/10.5194/acp-17-4419-2017,
522 2017.
523 Gysel, M., Crosier, J., Topping, D. O., Whitehead, J. D., Bower, K. N., Cubison, M. J., Williams, P. I.,
524 Flynn, M. J., McFiggans, G. B., and Coe, H.: Closure study between chemical composition and
525 hygroscopic growth of aerosol particles during TORCH2, Atmos. Chem. Phys., 7, 6131-6144,
526 doi:https://doi.org/10.5194/acp-7-6131-2007, 2007.
527 Huang, S., Wu, Z. J., Poulain, L., van Pinxteren, M., Merkel, M., Assmann, D., Herrmann, H., and
528 Wiedensohler, A.: Source apportionment of the organic aerosol over the Atlantic Ocean from 53 degrees
529 N to 53 degrees S: significant contributions from marine emissions and long-range transport, Atmos.
530 Chem. Phys., 18, 18043-18062,doi: 10.5194/acp-18-18043-2018, 2018
531 Huang, S., Wu, Z., Wang, Y., Poulain, L., Höpner, F., Merkel, M., Herrmann, H., and Wiedensohler, A.:
532 Aerosol Hygroscopicity and its Link to Chemical Composition in a Remote Marine Environment Based
533 on Three Transatlantic Measurements, Environ. Sci. Technol, 56, 9613-9622,
534 doi:https://doi.org/10.1021/acs.est.2c00785, 2022.
535 Ipcc: Annex I: Observational Products [Trewin, B. (ed.)], in: Climate Change 2021: The Physical Science
536 Basis. Contribution of Working Group I to the Sixth Assessment Report of the Intergovernmental Panel
537 on Climate Change, edited by: Masson-Delmotte, V., Zhai, P., Pirani, A., Connors, S. L., Péan, C., Berger,
538 S., Caud, N., Chen, Y., Goldfarb, L., Gomis, M. I., Huang, M., Leitzell, K., Lonnoy, E., Matthews, J. B.
539 R., Maycock, T. K., Waterfield, T., Yelekçi, O., Yu, R., and Zhou, B., Cambridge University Press,
540 Cambridge, United Kingdom and New York, NY, USA, 2061–2086,
541 https://doi.org/10.1017/9781009157896.015, 2021.
542 Jimenez, J. L., Canagaratna, M. R., Donahue, N. M., Prevot, A. S., Zhang, Q., Kroll, J. H., DeCarlo, P.
543 F., Allan, J. D., Coe, H., Ng, N. L., Aiken, A. C., Docherty, K. S., Ulbrich, I. M., Grieshop, A. P., Robinson,
544 A. L., Duplissy, J., Smith, J. D., Wilson, K. R., Lanz, V. A., Hueglin, C., Sun, Y. L., Tian, J., Laaksonen,
545 A., Raatikainen, T., Rautiainen, J., Vaattovaara, P., Ehn, M., Kulmala, M., Tomlinson, J. M., Collins, D.

546 R., Cubison, M. J., Dunlea, E. J., Huffman, J. A., Onasch, T. B., Alfarra, M. R., Williams, P. I., Bower,
547 K., Kondo, Y., Schneider, J., Drewnick, F., Borrmann, S., Weimer, S., Demerjian, K., Salcedo, D., Cottrell,
548 L., Griffin, R., Takami, A., Miyoshi, T., Hatakeyama, S., Shimono, A., Sun, J. Y., Zhang, Y. M., Dzepina,
549 K., Kimmel, J. R., Sueper, D., Jayne, J. T., Herndon, S. C., Trimborn, A. M., Williams, L. R., Wood, E.
550 C., Middlebrook, A. M., Kolb, C. E., Baltensperger, U., and Worsnop, D. R.: Evolution of organic
551 aerosols in the atmosphere, Science, 326, 1525-1529, doi:https://doi.org/10.1126/science.1180353, 2009.
552 Kawana, K., Miyazaki, Y., Omori, Y., Tanimoto, H., Kagami, S., Suzuki, K., Yamashita, Y., Nishioka, J.,
553 Deng, Y. G., Yai, H., and Mochida, M.: Number-Size Distribution and CCN Activity of Atmospheric
554 Aerosols in the Western North Pacific During Spring Pre-Bloom Period: Influences of Terrestrial and
555 Marine Sources, J Geophys Res-Atmos, 127, e2022JD036690,
556 doi:https://doi.org/10.1029/2022JD036690, 2022.
557 Köhler, H.: The nucleus in and the growth of hygroscopic droplets, Trans. Faraday Soc., 32, 1152-1161,
558 doi:https://doi.org/10.1039/TF9363201152, 1936.
559 Lambe, A. T., Onasch, T. B., Massoli, P., Croasdale, D. R., Wright, J. P., Ahern, A. T., Williams, L. R.,
560 Worsnop, D. R., Brune, W. H., and Davidovits, P.: Laboratory studies of the chemical composition and
561 cloud condensation nuclei (CCN) activity of secondary organic aerosol (SOA) and oxidized primary
562 organic aerosol (OPOA), Atmos. Chem. Phys., 11, 8913-8928, doi:https://doi.org/10.5194/acp-11-8913-
563 2011, 2011.
564 Leena, P. P., Pandithurai, G., Anilkumar, V., Murugavel, P., Sonbawne, S. M., and Dani, K. K.: Seasonal
565 variability in aerosol, CCN and their relationship observed at a high altitude site in Western Ghats,
566 Meteorol Atmos Phys, 128, 143-153, doi:https://doi.org/10.1007/s00703-015-0406-0, 2016.
567 Liang, B., Cai, M., Sun, Q., Zhou, S., and Zhao, J.: Source apportionment of marine atmospheric aerosols
568 in northern South China Sea during summertime 2018, Environ. Pollut, 289, 117948,
569 doi:https://doi.org/10.1016/j.envpol.2021.117948, 2021.
570 Liu, P., Song, M., Zhao, T., Gunthe, S. S., Ham, S., He, Y., Qin, Y. M., Gong, Z., Amorim, J. C., Bertram,
571 A. K., and Martin, S. T.: Resolving the mechanisms of hygroscopic growth and cloud condensation nuclei
572 activity for organic particulate matter, Nat. Commun, 9, 4076, doi:https://doi.org/10.1038/s41467-018-
573 06622-2, 2018.
574 Liu, X. and Wang, J.: How important is organic aerosol hygroscopicity to aerosol indirect forcing?,
575 Environ. Res. Lett, 5, 044010, doi:https://doi.org/10.1088/1748-9326/5/4/044010, 2010.

576 Liu, Y., Sun, L., Zhou, X., Luo, Y., Huang, W., Yang, C., Wang, Y., and Huang, T.: A 1400-year
577 terrigenous dust record on a coral island in South China Sea, Sci Rep, 4, 4994,
578 doi:https://doi.org/10.1038/srep04994, 2014.
579 Lu, W., Yang, S., Zhu, W., Li, X., Cui, S., Luo, T., Han, L., and Shi, J.: Evaluation of High Cloud Product
580 of ECMWF Over South China Sea Using CALIOP, Earth Space Sci, 9, e2021EA002113,
581 doi:https://doi.org/10.1029/2021ea002113, 2022.
582 Meng, J. W., Yeung, M. C., Li, Y. J., Lee, B. Y. L., and Chan, C. K.: Size-resolved cloud condensation
583 nuclei (CCN) activity and closure analysis at the HKUST Supersite in Hong Kong, Atmos. Chem. Phys.,
584 14, 10267-10282, doi:https://doi.org/10.5194/acp-14-10267-2014, 2014.
585 Moore, R. H., Nenes, A., and Medina, J.: Scanning Mobility CCN Analysis-A Method for Fast
586 Measurements of Size-Resolved CCN Distributions and Activation Kinetics, Aerosol Sci Tech, 44, 861-
587 871, doi:https://doi.org/10.1080/02786826.2010.498715, 2010.
588 Ou, H., Cai, M., Zhang, Y., Ni, X., Liang, B., Sun, Q., Mai, S., Sun, C., Zhou, S., Wang, H., Sun, j., and
589 Zhao, J.: Measurement Report: Seasonal variation and anthropogenic influence on cloud condensation
590 nuclei (CCN) activity in the South China Sea: Insights from shipborne observations during summer and
591 winter of 2021 [dataset], doi:https://doi.org/10.6084/m9.figshare.25472545, 2024.
592 Ovadnevaite, J., Zuend, A., Laaksonen, A., Sanchez, K. J., Roberts, G., Ceburnis, D., Decesari, S.,
593 Rinaldi, M., Hodas, N., Facchini, M. C., Seinfeld, J. H., and O' Dowd, C.: Surface tension prevails over
594 solute effect in organic-influenced cloud droplet activation, Nature, 546, 637-641,
595 doi:https://doi.org/10.1038/nature22806, 2017.
596 Patel, P. N. and Jiang, J. H.: Cloud condensation nuclei characteristics at the Southern Great Plains site:
597 role of particle size distribution and aerosol hygroscopicity, Environ Res Commun, 3,
598 doi:https://doi.org/10.1088/2515-7620/ac0e0b, 2021
599 Petters, M. D. and Kreidenweis, S. M.: A single parameter representation of hygroscopic growth and
600 cloud condensation nucleus activity, Atmos. Chem. Phys., 7, 1961-1971, doi:https://doi.org/10.5194/acp-
601 7-1961-2007, 2007.
602 Pöhlker, M. L., Pöhlker, C., Ditas, F., Klimach, T., Hrabe de Angelis, I., Araújo, A., Brito, J., Carbone,
603 S., Cheng, Y., Chi, X., Ditz, R., Gunthe, S. S., Kesselmeier, J., Könemann, T., Lavrič, J. V., Martin, S. T.,
604 Mikhailov, E., Moran-Zuloaga, D., Rose, D., Saturno, J., Su, H., Thalman, R., Walter, D., Wang, J., Wolff,
605 S., Barbosa, H. M. J., Artaxo, P., Andreae, M. O., and Pöschl, U.: Long-term observations of cloud

606 condensation nuclei in the Amazon rain forest – Part 1: Aerosol size distribution, hygroscopicity, and
607 new model parametrizations for CCN prediction, Atmos. Chem. Phys., 16, 15709-15740,
608 doi:https://doi.org/10.5194/acp-16-15709-2016, 2016.
609 Qin, Y., Wang, H., Wang, Y., Lu, X., Tang, H., Zhang, J., Li, L., and Fan, S.: Wildfires in Southeast Asia
610 pollute the atmosphere in the northern South China Sea, Sci Bull (Beijing), 69, 1011-1015,
611 doi:https://doi.org/10.1016/j.scib.2024.02.026, 2024.
612 Quinn, P. K., Bates, T. S., Coffman, D. J., and Covert, D. S.: Influence of particle size and chemistry on
613 the cloud nucleating properties of aerosols, Atmos. Chem. Phys., 8, 1029-1042,
614 doi:https://doi.org/10.5194/acp-8-1029-2008, 2008.
615 Quinn, P. K., Bates, T. S., Coffman, D. J., Upchurch, L., Johnson, J. E., Moore, R., Ziemba, L., Bell, T.
616 G., Saltzman, E. S., Graff, J., and Behrenfeld, M. J.: Seasonal Variations in Western North Atlantic
617 Remote Marine Aerosol Properties, J Geophys Res-Atmos, 124, 14240-14261,
618 doi:https://doi.org/10.1029/2019jd031740, 2019.
619 Rose, D., Nowak, A., Achtert, P., Wiedensohler, A., Hu, M., Shao, M., Zhang, Y., Andreae, M. O., and
620 Poschl, U.: Cloud condensation nuclei in polluted air and biomass burning smoke near the mega-city
621 Guangzhou, China - Part 1: Size-resolved measurements and implications for the modeling of aerosol
622 particle hygroscopicity and CCN activity, Atmos. Chem. Phys., 10, 3365-3383,
623 doi:https://doi.org/10.5194/acp-10-3365-2010, 2010.
624 Ross, K. E., Piketh, S. J., Bruintjes, R. T., Burger, R. P., Swap, R. J., and Annegarn, H. J.: Spatial and
625 seasonal variations in CCN distribution and the aerosol-CCN relationship over southern Africa, J
626 Geophys Res-Atmos, 108, doi:https://doi.org/10.1029/2002jd002384, 2003.
627 Safai, P. D., Raju, M. P., Rao, P. S. P., and Pandithurai, G.: Characterization of carbonaceous aerosols
628 over the urban tropical location and a new approach to evaluate their climatic importance, Atmos Environ,
629 92, 493-500, doi:https://doi.org/10.1016/j.atmosenv.2014.04.055, 2014.
630 Sarangi, B., Ramachandran, S., Rajesh, T. A., and Dhaker, V. K.: Black carbon linked aerosol hygroscopic
631 growth: Size and mixing state are crucial, Atmos Environ., 200, 110-118,
632 doi:https://doi.org/https://doi.org/10.1016/j.atmosenv.2018.12.001, 2019.
633 Schmale, J., Henning, S., Decesari, S., Henzing, B., Keskinen, H., Sellegri, K., Ovadnevaite, J., Pohlker,
634 M. L., Brito, J., Bougiatioti, A., Kristensson, A., Kalivitis, N., Stavroulas, I., Carbone, S., Jefferson, A.,
635 Park, M., Schlag, P., Iwamoto, Y., Aalto, P., Aijala, M., Bukowiecki, N., Ehn, M., Frank, G., Frohlich, R.,

Frumau, A., Herrmann, E., Herrmann, H., Holzinger, R., Kos, G., Kulmala, M., Mihalopoulos, N., Nenes, A., O'Dowd, C., Petaja, T., Picard, D., Pohlker, C., Poschl, U., Poulain, L., Prevot, A. S. H., Swietlicki, E., Andreae, M. O., Artaxo, P., Wiedensohler, A., Ogren, J., Matsuki, A., Yum, S. S., Stratmann, F., Baltensperger, U., and Gysel, M.: Long-term cloud condensation nuclei number concentration, particle number size distribution and chemical composition measurements at regionally representative observatories, Atmos. Chem. Phys., 18, 2853-2881, doi:https://doi.org/10.5194/acp-18-2853-2018, 2018.

Seinfeld, J. H. and Pandis, S. N.: Atmospheric Chemistry and Physics: From Air Pollution to Climate Change, Wiley2016.

Sihto, S. L., Mikkila, J., Vanhanen, J., Ehn, M., Liao, L., Lehtipalo, K., Aalto, P. P., Duplissy, J., Petaja, T., Kerminen, V. M., Boy, M., and Kulmala, M.: Seasonal variation of CCN concentrations and aerosol activation properties in boreal forest, Atmos. Chem. Phys., 11, 13269-13285, doi:https://doi.org/10.5194/acp-11-13269-2011, 2011.

Sun, Q., Liang, B., Cai, M., Zhang, Y., Ou, H., Ni, X., Sun, X., Han, B., Deng, X., Zhou, S., and Zhao, J.: Cruise observation of the marine atmosphere and ship emissions in South China Sea: Aerosol composition, sources, and the aging process, Environ. Pollut, 316, 120539, doi:https://doi.org/10.1016/j.envpol.2022.120539, 2023.

Wang, B., Huang, F., Wu, Z., Yang, J., Fu, X., and Kikuchi, K.: Multi-scale climate variability of the South China Sea monsoon: A review, Dynam Atmos Oceans, 47, 15-37, doi:https://doi.org/10.1016/j.dynatmoce.2008.09.004, 2009.Wang, Y., Chen, J., Wang, Q., Qin, Q., Ye, J., Han, Y., Li, L., Zhen, W., Zhi, Q., Zhang, Y., and Cao, J.: Increased secondary aerosol contribution and possible processing on polluted winter days in China, Environ Int, 127, 78-84, doi:https://doi.org/10.1016/j.envint.2019.03.021, 2019.

Wang, Y. Q.: MeteoInfo: GIS software for meteorological data visualization and analysis, Meteorol. Appl, 21, 360-368, doi:https://doi.org/10.1002/met.1345, 2014.

Xiao, H.-W., Xiao, H.-Y., Luo, L., Shen, C.-Y., Long, A.-M., Chen, L., Long, Z.-H., and Li, D.-N.: Atmospheric aerosol compositions over the South China Sea: temporal variability and source apportionment, Atmos. Chem. Phys., 17, 3199-3214, doi:https://doi.org/10.5194/acp-17-3199-2017, 2017.

664 Table 1. The number concentration of particle and cloud condensation nuclei at different supersaturation (SS), the hygroscopicity and activation ratio (AR) at different SS in
665 different studies.

Location	period	N_{CN} (cm^{-3})	N_{CCN} (cm^{-3})	Hygroscopicity (κ)	AR	Reference
South China Sea	2021.05.05-2021.06.09	6966±9249	2019±2993 (0.20% SS) 4445±7018 (0.40% SS) 4786±6402 (0.70% SS)	0.49±0.42 (0.20% SS) 0.74±0.51 (0.40% SS)	0.43±0.17 (0.20% SS) 0.68±0.19 (0.40% SS) 0.89±0.12 (0.70% SS)	This study
Northern South China Sea	2021.12.19-2021.12.29	4988±3474	1100±1287 (0.10% SS) 1678±1046 (0.20% SS) 2346±1767 (0.40% SS) 2921±1917 (0.70% SS)	0.50±0.21 (0.10% SS) 0.31±0.10 (0.20% SS) 0.19±0.05 (0.40% SS) 0.15±0.05 (0.70% SS)	0.23±0.10 (0.10% SS) 0.35±0.12 (0.20% SS) 0.48±0.14 (0.40% SS) 0.60±0.16 (0.70% SS)	This study
Northern South China Sea	2018.8.6-2018.8.27	3463	1544 (0.34% SS)	0.38±0.09 (0.18% SS) 0.40±0.08 (0.34% SS) 0.38±0.08 (0.59% SS)	/	Cai et al., 2020
Remote South China Sea	2012.9.14-2012.9.26	503±455	450±388 (0.14% SS) 675±516 (0.38% SS) 698±555 (0.53% SS) 724±512 (0.71% SS)	0.54±0.14 (0.14% SS) 0.50±0.21 (0.38% SS)	0.47±0.16 (0.14% SS) 0.72±0.17 (0.38% SS) 0.79±0.15 (0.53% SS) 0.85±0.13 (0.71% SS)	Atwood et al., 2017
Western North Pacific	2015.3.4-2015.3.26	/	/	0.75±0.21 (0.11% SS) 0.51±0.16 (0.24% SS) 0.45±0.16 (0.60% SS)	0.40±0.22 (0.11% SS) 0.50±0.22 (0.24% SS) 0.70±0.23 (0.60% SS)	Kawana et al., 2020
Guangzhou	2014.11-2014.12	/	3103±1913 (0.10% SS) 5095±2972 (0.20% SS) 6524±3783 (0.40% SS)	0.37±0.11 (0.10% SS) 0.29±0.09 (0.20% SS) 0.18±0.07 (0.40% SS)	0.26±0.10 (0.10% SS) 0.41±0.14 (0.20% SS) 0.53±0.15 (0.40% SS)	Cai et al., 2018

	7913±4234 (0.70% SS)	0.15±0.06 (0.70% SS)	0.64±0.13 (0.70% SS)

666

667 Table 2. The number concentration of particle and cloud condensation nuclei in different periods.

	Summer			Winter		
Cluster	Indochinese Peninsula	Luzon	Marine	Mainland China	Marine	Mixed
N_{CCN} (cm^{-3})						
0.1% SS	\	\	\	1460±1670	464±243	929±444
0.2% SS	1290±785	4093±4864	1112±682	2105±974	649±362	1499±548
0.4% SS	1634±1121	8241±7478	1885±1142	3014±1934	831±439	1900±696
0.7% SS	1968±1111	10776±10540	2477±1541	3668±1841	1052±493	2296±829
N_{CN} (cm^{-3})						
Total	2699±2147	14674±13844	3033±2366	6875±3263	1728±465	2918±1204
Nucleation	111±206	1543±3341	238±426	893±925	214±281	141±191
Aikten	1156±1261	8653±8815	1668±1526	3089±2017	732±337	806±427
Accumulation	1434±1444	3764±4157	1121±929	2923±2440	781±313	1975±831

668

669

Table 3. The slope and coefficient of determination (in parentheses) in CCN closure analysis at different supersaturations in different periods.

	Summer			Winter		
Cluster	Luzon	Indochinese Peninsula	Marine	Mainland China	Mixed	Marine
Internal scheme						
0.1% SS	\	\	\	0.81 (0.94)	0.64 (0.92)	0.65 (0.95)
0.2% SS	0.82 (0.82)	0.73 (0.80)	0.79 (0.91)	1.05 (0.96)	0.93 (0.97)	0.79 (0.89)
0.4% SS	0.79 (0.92)	0.76 (0.62)	0.80 (0.92)	1.23 (0.97)	1.04 (0.98)	1.01 (0.95)
0.7% SS	0.80 (0.88)	0.85 (0.52)	0.80 (0.90)	1.26 (0.97)	1.06 (0.99)	0.97 (0.91)
External scheme						
0.1% SS	\	\	\	0.97 (0.95)	0.96 (0.92)	0.97 (0.95)
0.2% SS	0.73 (0.83)	0.63 (0.76)	0.75 (0.90)	0.98 (0.96)	0.99 (0.97)	0.94 (0.89)
0.4% SS	0.69 (0.85)	0.69 (0.65)	0.74 (0.91)	0.99 (0.97)	0.99 (0.98)	0.97 (0.95)
0.7% SS	0.70 (0.85)	0.80 (0.53)	0.72 (0.88)	0.99 (0.97)	0.99 (0.99)	0.96 (0.92)

674 FIGURE CAPTION

675 Figure 1. The cruises of two shipborne observations, and the location of sample line and chimney of Tan
676 Kah Kee, and Sun Yat-sen scientific vessel (a); Wind rose of the wind direction and wind speed in
677 summer and winter cruises; The radius represents the frequency of wind direction occurrences, and the
678 shaded areas indicate wind speed (b) and (c).

679 Figure 2. Timeseries of (a) particle number size distribution, (b) mass concentration of NR-PM_1, and (c)
680 its fraction, (d) mass concentration of organic carbon and elemental carbon, (e) number concentration of
681 total particle and cloud condensation nuclei under the supersaturation of 0.1%, 0.2%, 0.4%, and 0.7%,
682 and (f) aerosol hygroscopicity. The number 1 in figure number means timeseries in summer and number
683 2 means it in winter.

684 Figure 3. Particle number size distribution in summer (a) and winter (b); The red markers represent the
685 activation diameters and hygroscopicity parameters corresponding to 0.1%, 0.2%, 0.4%, and 0.7%
686 supersaturations in this study (without 0.1% in summer). The green markers represent the hygroscopicity
687 parameters reported in Atwood et al. (2017) for the southern South China Sea during summer. The gray
688 markers represent the hygroscopicity parameters documented in Cai et al. (2018) for the Pearl River
689 Delta region during winter. The fraction of NR-PM_1 in summer (c) and winter (d) in this study, in northern
690 SCS reported by Liang et al. (2021) (e), and in North Pacific reported by Choi et al. (2017) (f).

691 Figure 4. The cluster analysis result in summer (a), and winter (b). The solid line in summer means cluster
692 analysis from May 5 to May 24 and the dash line in summer means cluster analysis from May 25 to June
693 9; The solid line in winter means cluster analysis from Dec 19 to Dec 21 and Dec 27 to Dec 29, and the
694 dash line in winter means cluster analysis from Dec 22 to Dec 26.

695 Figure 5. The fraction of NR-PM_1 in “Luzon” period (a), “Indochinese Peninsula" period (b), and
696 “Marine-s” period (c) in summer. The fraction of NR-PM_1 in “Mainland China” period (d), “Mixed"
697 period (e), and “Marine-w” period (f) in winter.

698 Figure 6. The particle number size distribution (PNSD) in “Luzon” period (a), “Indochinese Peninsula"
699 period (b), and “Marine-s” period (c) in summer. The PNSD in “Mainland China” period (d), “Mixed"
700 period (e), and “Marine-w” period (f) in winter.

701 Figure 7. The activation ratio (AR) at different supersaturation (SS) in different periods (a); The
702 aerosol hygroscopicity (κ) at different supersaturation (SS) in different periods (b).

Figure 8. The normalized mean bias (NMB) calculated by “Internal-mixed” scheme and “External-mixed” scheme according to CCN closure method. The marker of circle means “Internal-mixed” scheme and the marker of triangle means “External-mixed” scheme. Different colors means different supersaturations.

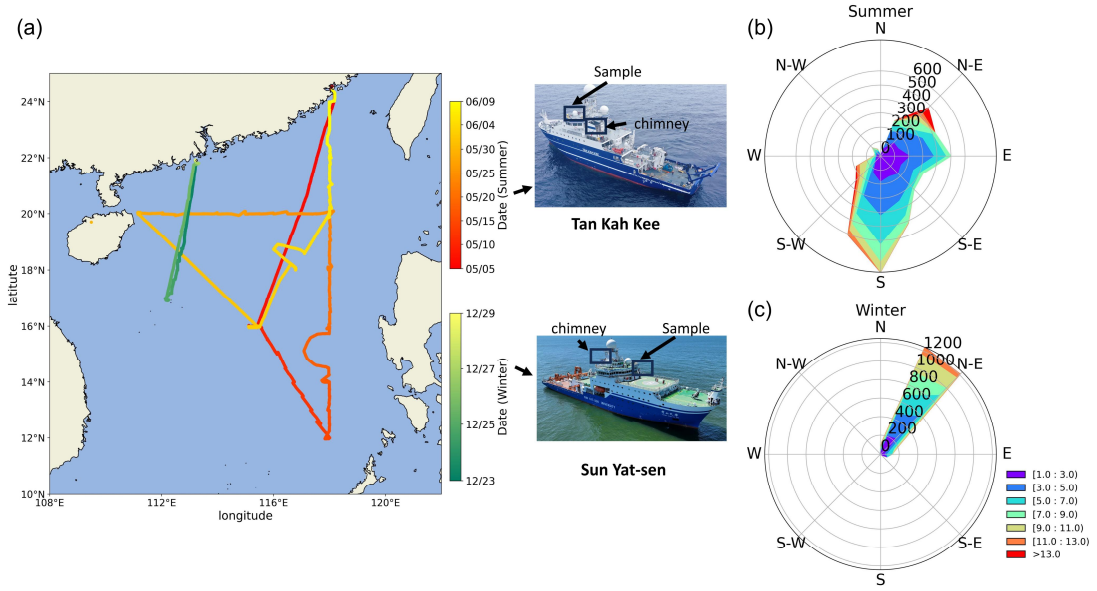
(a)
24°N
22°N
20°N
18°N
16°N
14°N
12°N
10°N
108°E
112°E
116°E
120°E
longitude
latitute
06/09
06/04
05/30
05/25
05/20
05/15
05/10
05/05
Date (Summer)
12/29
12/27
12/25
12/23
Date (Winter)
Sample
chimney
Tan Kah Kee
chimney
Sample
Sun Yat-sen
(b)
Summer
N
N-E
E
S-E
S
S-W
W
N-W
600
500
400
300
200
100
0
(c)
Winter
1200
1000
800
600
400
200
[1.0 : 3.0)
[3.0 : 5.0)
[5.0 : 7.0)
[7.0 : 9.0)
[9.0 : 11.0)
[11.0 : 13.0)
>13.0

Fig. 1

712

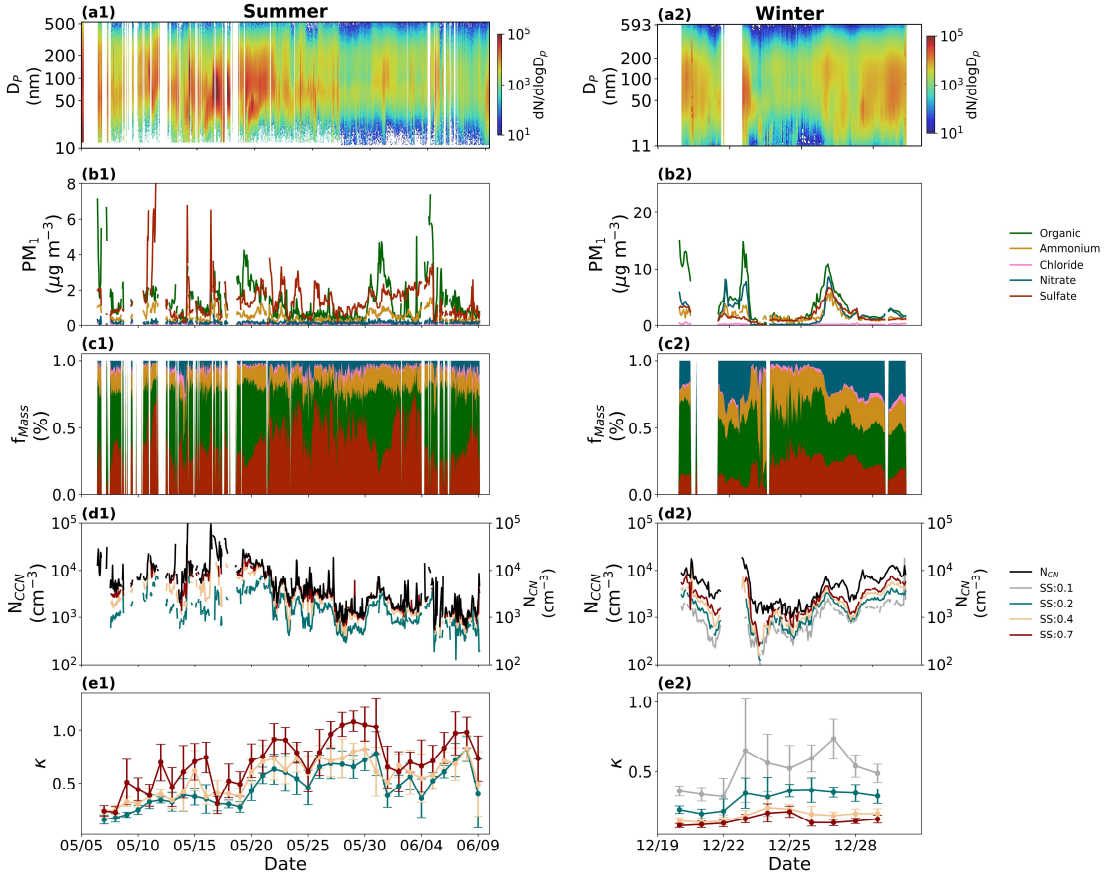

713

714 Fig. 2

715

716

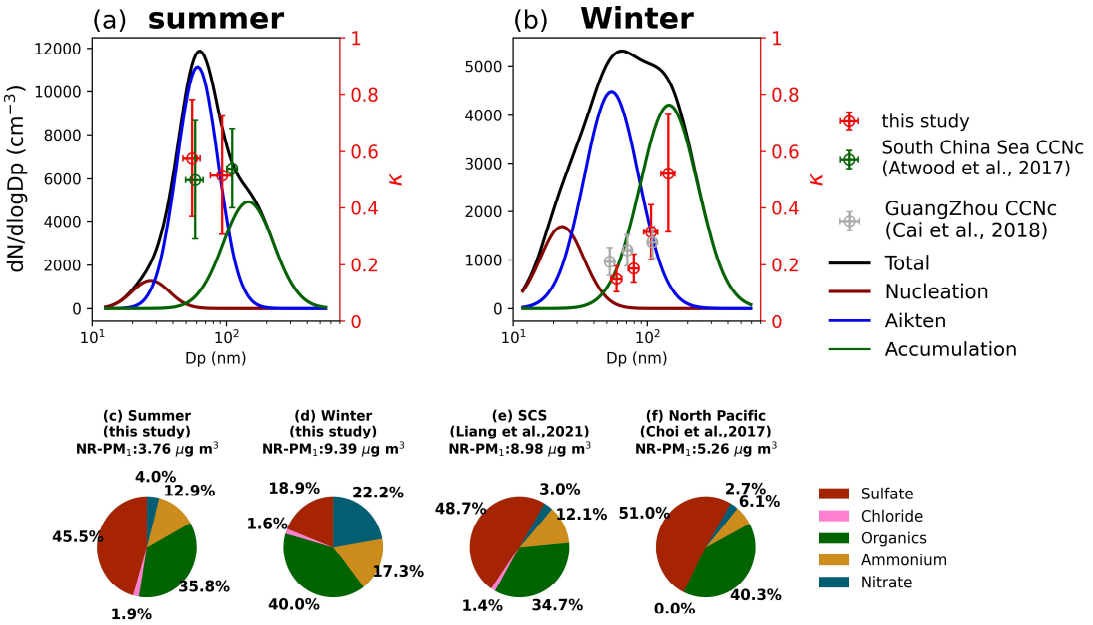

717

718 Fig. 3

719

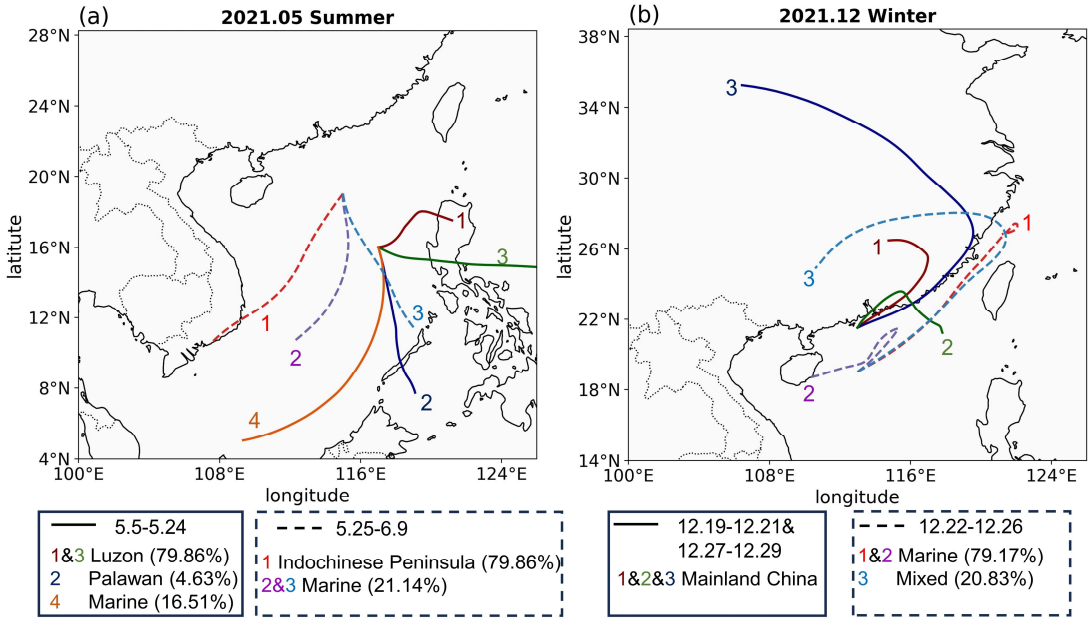
(a)
2021.05 Summer
(b)
2021.12 Winter
latitude
longitude
28°N
24°N
20°N
16°N
12°N
8°N
4°N
38°N
34°N
30°N
26°N
22°N
18°N
14°N
100°E
108°E
116°E
124°E
5.5-5.24
1&3 Luzon (79.86%)
2 Palawan (4.63%)
4 Marine (16.51%)
5.25-6.9
1 Indochinese Peninsula (79.86%)
2&3 Marine (21.14%)
12.19-12.21&
12.27-12.29
1&2&3 Mainland China
12.22-12.26
1&2 Marine (79.17%)
3 Mixed (20.83%)

Fig. 4

723

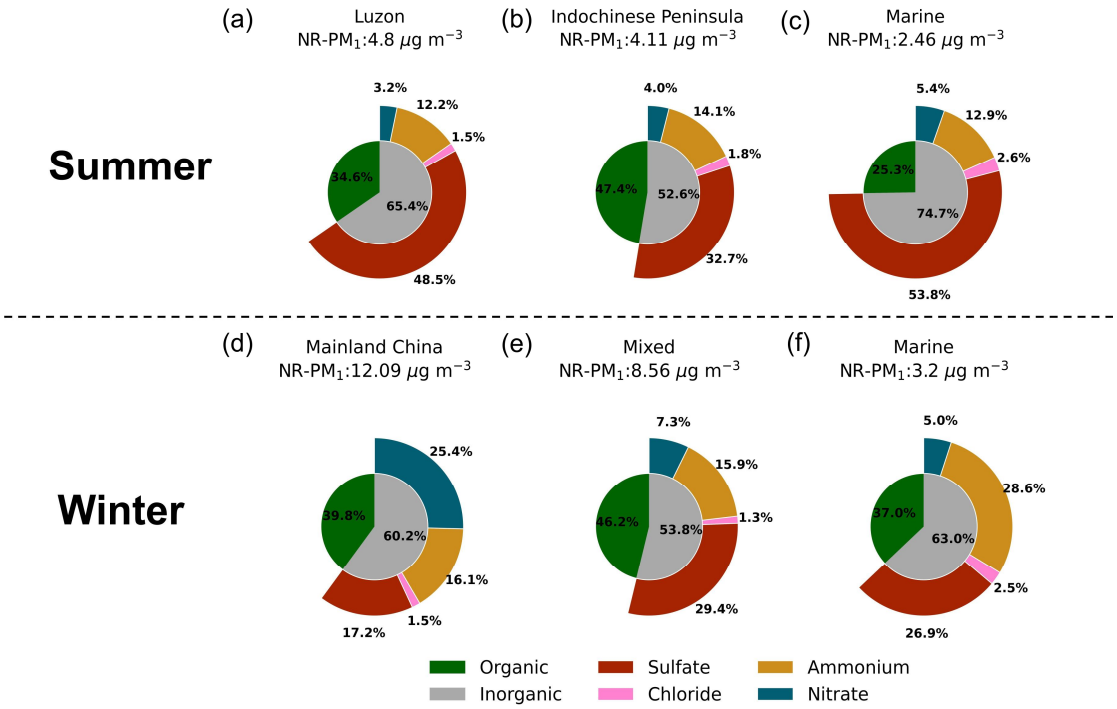

724

725 Fig.5

726

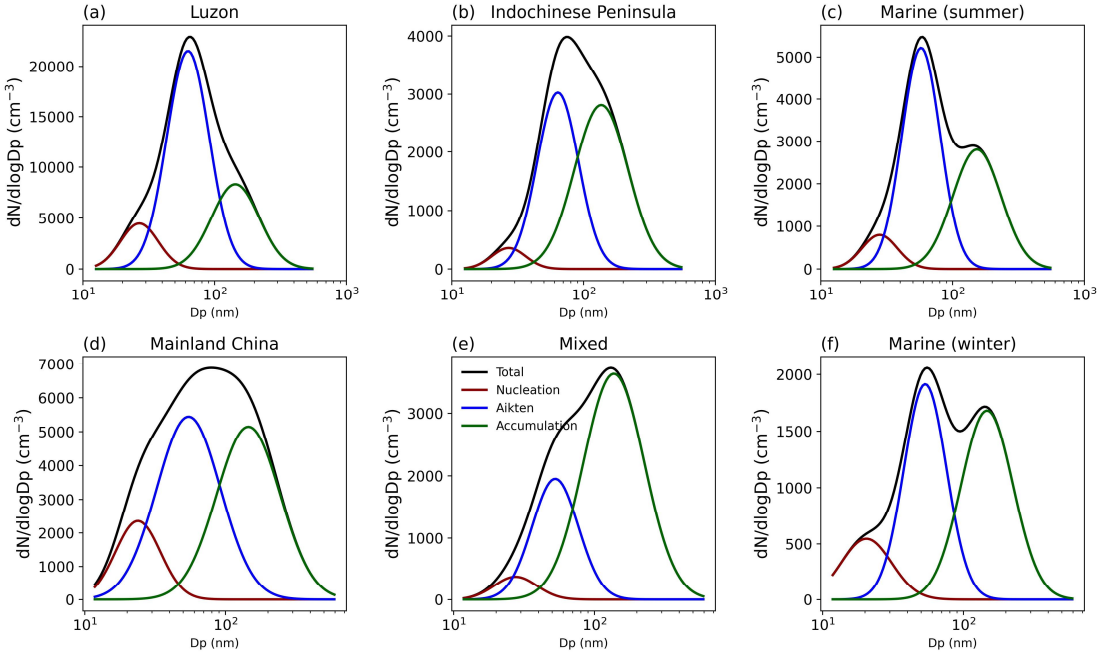
(a) Luzon
(b) Indochinese Peninsula
(c) Marine (summer)
(d) Mainland China
(e) Mixed
(f) Marine (winter)
Total
Nucleation
Aikten
Accumulation
dN/dlogDp (cm^{-3})
Dp (nm)

Fig. 6

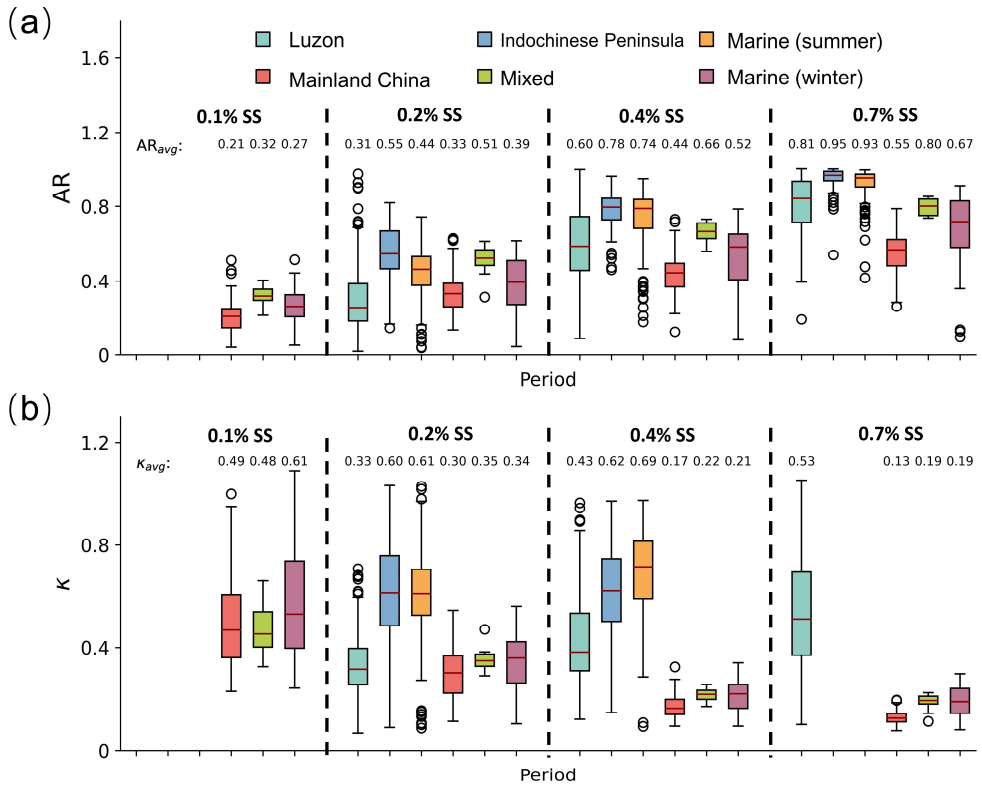
(a)
Luzon
Indochinese Peninsula
Marine (summer)
Mainland China
Mixed
Marine (winter)
0.1% SS
0.2% SS
0.4% SS
0.7% SS
AR_avg:
0.21 0.32 0.27
0.31 0.55 0.44 0.33 0.51 0.39
0.60 0.78 0.74 0.44 0.66 0.52
0.81 0.95 0.93 0.55 0.80 0.67
AR
Period
(b)
κ_avg:
0.49 0.48 0.61
0.33 0.60 0.61 0.30 0.35 0.34
0.43 0.62 0.69 0.17 0.22 0.21
0.53
0.13 0.19 0.19
κ
Period

Fig. 7

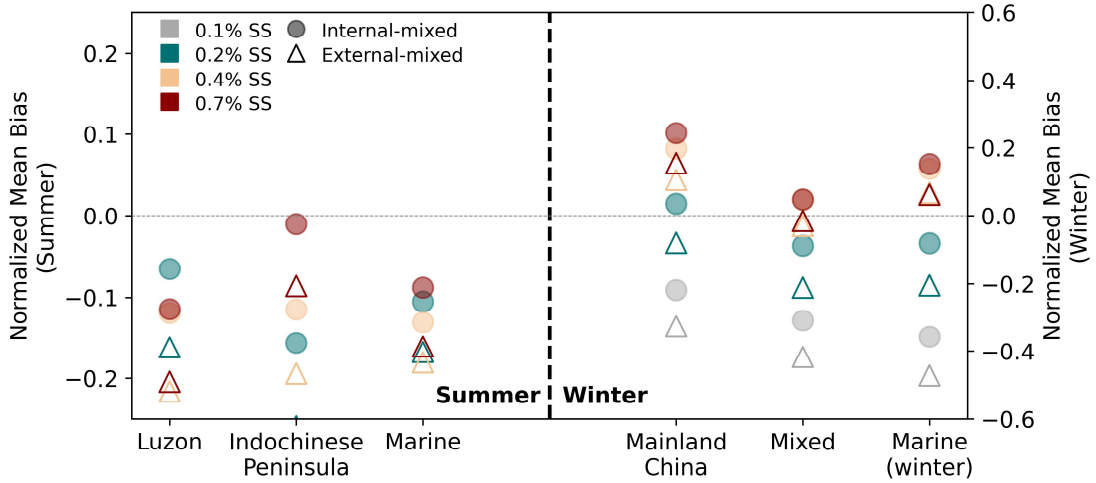

735

736 Fig. 8

737